ISSN 1063-7737, Astronomy Letters, 2011, Vol. 37, No. 8, pp. 563–575. © Pleiades Publishing, Inc., 2011.
Original Russian Text © S.A. Khoperskov, A.V. Khoperskov, M.A. Eremin, M.A. Butenko, 2011, published in Pis'ma v Astronomicheskiĭ Zhurnal, 2011, Vol. 37, No. 8, pp. 614–627.

Polygonal Structures in a Gaseous Disk: Numerical Simulations

S. A. Khoperskov*, A. V. Khoperskov, M. A. Eremin, and M. A. Butenko**

Volgograd State University, Vtoraya Prodolnaya ul. 30, Volgograd, 400062 Russia

Received February 1, 2011

Abstract—The results of numerical simulations of a gaseous disk in the potential of a stellar spiral density wave are presented. The conditions under which straightened spiral arm segments (rows) form in the gas component are studied. These features of the spiral structure were identified in a series of works by A.D. Chernin with coauthors. Gas-dynamic simulations have been performed for a wide range of model parameters: the pitch angle of the spiral pattern, the amplitude of the stellar spiral density wave, the disk rotation speed, and the temperature of the gas component. The results of 2D- and 3D-disk simulations are compared. The rows in the numerical simulations are shown to be an essentially nonstationary phenomenon. A statistical analysis of the distribution of geometric parameters for spiral patterns with rows in the observed galaxies and the constructed hydrodynamic models shows good agreement. In particular, the numerical simulations and observations of galaxies give $\langle\alpha\rangle \simeq 120^\circ$ for the average angles between straight segments.

DOI: 10.1134/S032001081108002X

Keywords: *numerical gas dynamics, shock waves, spiral structure of galaxies.*

PECULIARITIES OF OBSERVED SPIRAL PATTERNS

The Geometric Shape of Spiral Structures

Smooth regular spiral arms in grand-design galaxies are encountered very rarely. As a rule, the global spiral pattern is characterized by a large number of various inhomogeneities on small and medium spatial scales: spurs (Elmegreen 1980; Chakrabarti et al. 2003; Shetty and Ostriker 2006; Muraoka et al. 2009), feathers (Dobbs and Bonnell 2006; La Vigne et al. 2006), branchings and branch thickenings, and quasi-periodic complexes along the arms (Efremov and Chernin 2003; Efremov 2009). Interestingly, the small-scale inhomogeneity along the azimuth angle is also pronounced in ring structures, such as NGC 7742 and NGC 7217 (Silchenko and Moiseev 2006). The so-called rows or polygonal structures (PSs) by which we will mean the sequences of extended almost straight segments forming the spiral patterns of many galaxies (Waller et al. 1997; Pohlen and Trujillo 2006) are larger-scale features of the spiral pattern. Vorontsov-Vel'yaminov was the first to notice such objects, calling them rows (Vorontsov-Vel'yaminov 1964, 1977). In a series of works, Chernin with coauthors considered in detail the properties of PSs for nearby galaxies (Chernin 1998, 1999a; Chernin et al. 2000, 2001a) and our Galaxy (Chernin 1999b). There is evidence for the presence of straightened segments of the spital structure in M31 (Efremov 2001, 2009, 2010). The so-called "hexagonal" shape in some internal ring structures of galaxies may be similar in nature (Chernin et al. 2001b).

Polygonal structures are revealed not only in the optical range by young star clusters by also by the distribution of interstellar H I gas, dust, synchrotron emission, ultraviolet emission, and Hα. Meanwhile, the spiral arms formed by old stars appear smoother in infrared images of galaxies. Figure 1 schematically shows the PSs that we identified for a number of observed objects additional to the catalog by Chernin et al. (2001a).

Note the most characteristic features of polygonal structures from observational data (see Chernin 1998, 1999a, 1999b; Chernin et al. 2000, 2001a).

(1) For the sample of nearest galaxies constructed by Chernin et al. (2001a), the number of objects with PSs exceeds 200, which accounts for about 5–10% of the total number of galaxies with a global spiral structure.

(2) The average angle between neighboring straight segments from observational data is $\langle\alpha\rangle \simeq 120^\circ$ (Chernin et al. 2000). The scatter of values lies within the range $100^\circ \lesssim \alpha \lesssim 145^\circ$ (Chernin et al. 2001a). The length of such segments ℓ, on average, increases in direct proportion to the

*E-mail: shoperskov@gmail.com
**E-mail: khoperskov@volsu.ru

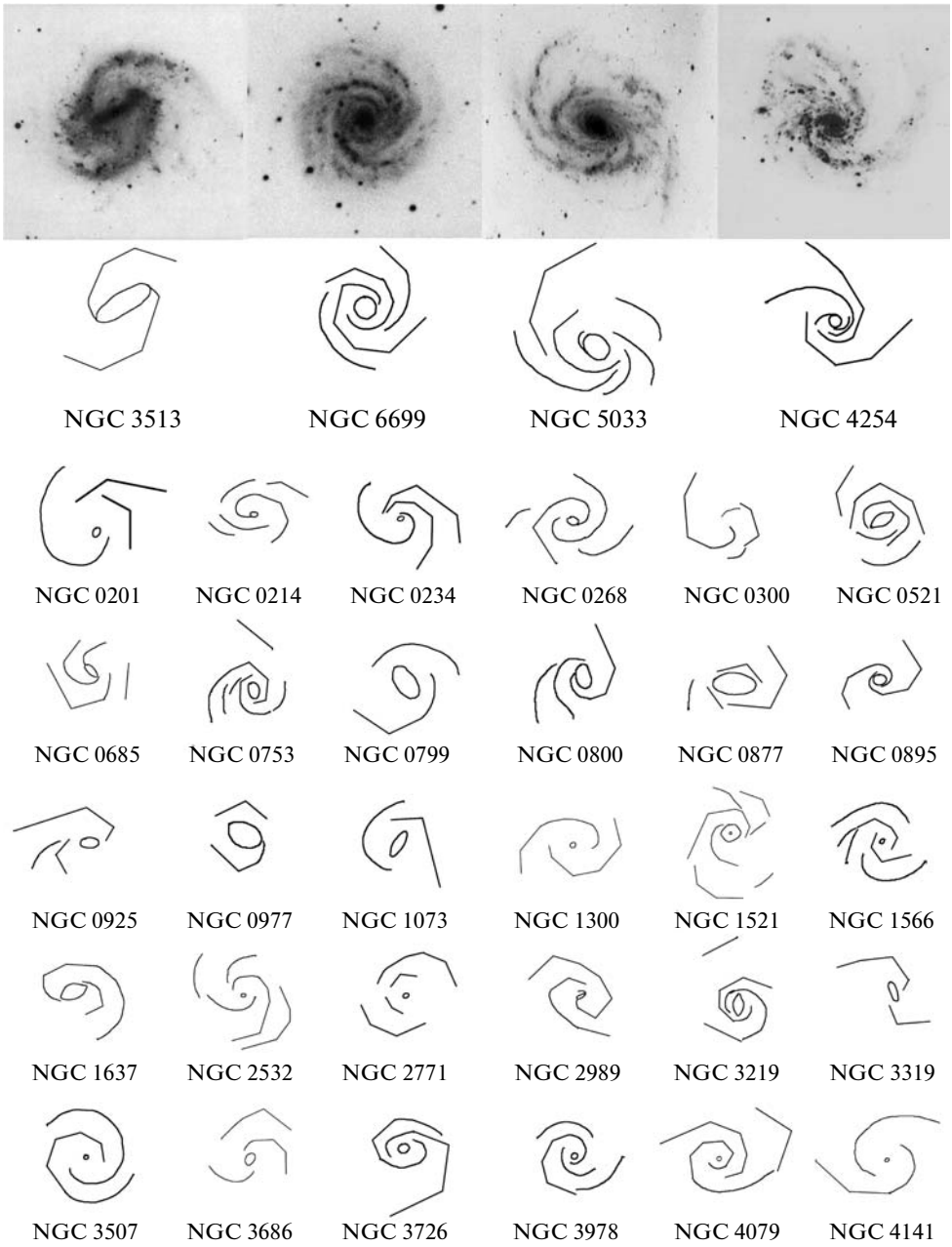

Fig. 1. New examples of the schematic view of galaxies with PSs additional to the data from Chernin et al. (2001a).

galactocentric distance d (Chernin 1999a; Chernin et al. 2001a).

(3) PSs are present both in SB galaxies and in systems without any central bar, but mostly in later-type objects (Sbc, Scd).

(4) The relative abundance of gas is significant, $M_{\rm HI}/L \simeq 0.15{-}0.4$ ($M_{\rm HI}/L$ is the mass-to-light ratio in solar units), but exceptions are possible, for example, this ratio for NGC 4548 is only $M_{\rm HI}/L \simeq 0.04$ (Chernin et al. 2000).

(5) The rotation speed estimates for the galaxies considered are not very reliable, because the disks are oriented almost face-on, but, on the whole, the maximum rotation speeds (in the plateau region) exceed 150 km s^{-1}.

(6) An enhanced fraction of interacting galaxies is observed among objects with PSs. The longest rows ($\ell \gtrsim 8$ kpc) are encountered mostly in interacting galaxies, while shorter rows ($\ell \lesssim 5$ kpc) are observed a factor of $\simeq$4 more often in galaxies without any apparent manifestations of interaction.

(7) The number of rows identified in various objects lies within the range $n_{\rm row} = 1{-}9$ and the mean number in the sample is 3 rows.

(8) Rows (kinks and straight segments) can be identified in some ring galaxies; Chernin et al. (2001c) called such systems hexagonal structures (e.g., NGC 7020, NGC 4429, NGC 3351, NGC 6782, NGC 6935, UGC 12646, ESO 325-28) (see also Buta and Combes 1996)).

Apart from galaxies with a large number of straight segments of spirals for both spiral arms, in several galaxies kinks can be identified only in one of the galactic arms (see NGC 4548 and NGC 7137, Chernin et al. 2000).

Several mechanisms have been proposed to explain the formation of straightened segments of galactic spiral arms. According to the hypothesis suggested by Contopoulous and Grosbol (1986), the presence of PSs is associated with the influence of resonance regions in the stellar population dynamics. Chernin (1999a) and Chernin et al. (2000) proposed an alternative mechanism for the formation of polygonal structures: the straightened segments of spirals result from the development of instability of the galactic shock front that leads to its fragmentation into flat areas. Indeed, based on 2D hydrodynamic simulations of a nonrotating gas, Chernin et al. (2006) showed that when the gas flows through a curved potential well, the front of a plane shock in the case of oblique onflow breaks up into individual fragments and the effect of shock escape from the potential well takes place.

Thus, the observed straightening of spiral segments in galaxies can be hydrodynamic in nature. Nevertheless, a number of physically important factors remained outside the scope of the numerical simulations described by Chernin et al. (2006), where the conclusion reached in models without rotation that the shock front is located at the flow entrance into the potential well of a stellar density wave seems to be the main shortcoming. Observational data point to the positions of the characteristic dust lanes associated with the shock opposite to those in Chernin et al. (2006). This manifests itself particularly clearly in barred galaxies when the corotation radius is near the ends of the stellar bar (see the images of NGC 1097, NGC 1300, NGC 1365). The dust lane lies at the leading edge inside the bar and at the trailing edge in the spirals outside the bar.

Barred Galaxies

Traditionally, the spiral pattern in SB galaxies is associated with a nonaxisymmetric perturbation of the central stellar bar (or oval). Until recently, under the assumption that the system is stationary, the kinematics of the spiral structure was believed to be determined by the rotation of a rigidly rotating bar with a pattern speed $\Omega_{\rm bar}$. If the corotation radius of the bar $r_c^{\rm bar}$ is near its ends, then the corotation of spirals is also nearby, $r_c^{\rm spir} \simeq r_c^{\rm bar}$. Thus, the solid-body rotation speed of the spiral pattern $\Omega_{\rm spir}$ is everywhere larger than the disk rotation speed $\Omega(r) = V(r)/r < \Omega_{\rm spir}$. Let us separately discuss the question about PSs in galaxies with a central bar/oval based on the OSUBGS sample of galaxies for which the corotation radii $r_{\rm c}$ were determined in a number of works (Rautiainen et al. 2008; Buta and Zhang 2009). A characteristic feature of the analysis performed by Buta and Zhang (2009) is the existence of an outer corotation radius $r_{\rm c}$ outside the apparent spiral structure $\mathcal{R} = r_{\rm c}/r_{\rm bar} \gtrsim 2$ for more than 60% of the galaxies. This points to slow rotation of at least the outer spiral arms, $\Omega_{\rm spir} < \Omega(r) = V/r$.

The estimated positions of the relative corotation radius $\mathcal{R} = r_{\rm c}/r_{\rm bar}$ for 38 SB galaxies from the OSUBGS sample in Rautiainen et al. (2008) show that $\mathcal{R} = r_{\rm c}/r_{\rm bar}$ exceeds appreciably unity for a sizeable fraction of the galaxies. We will point out NGC 0289, NGC 0578, NGC 1187, NGC 3726, NGC 4051, NGC 4995, and NGC 6384 with $\mathcal{R} = r_{\rm c}/r_{\rm bar} = 1.8$–$3.4$. Other examples of such objects are also known: $\mathcal{R}_{\rm NGC\ 3081} = 2.2$ (Buta and Purcell 1998) and $\mathcal{R}_{\rm NGC\ 0925} = 3.1$ (Elmegreen et al. 1998). Based on the results by Zhang and Buta (2007, 2010), we can identify the galaxies NGC 5194, NGC 5247, NGC 4321, NGC 4622, and NGC 1073 for which the outer corotation radius is outside the spiral structure or on its periphery. Analysis of the images for OSUBGS galaxies with $\mathcal{R} \gtrsim 2$ from the papers listed above shows that NGC 1187, NGC 1385, NGC 3513, NGC 3686, NGC 4145, NGC 4902, NGC 5194, NGC 5334, and NGC 7418 have rows. The existence of several corotation radii is an argument for the necessity of changing the common viewpoint on invariability of the morphological type and stationarity of the spiral pattern in the extreme case of a very slow change in the parameters of spirals in favor of faster transformations with characteristic times of the order of the revolution period.

Several corotation radii may also simultaneously exist in our Galaxy, which is indicative of nonstationary dynamics (Gerhard 2010, and references therein). Gerhard (2010) again draws attention to the old contradiction between a rapidly rotating bar with a pattern speed $\Omega_{\rm bar} \sim 59$ km s^{-1} kpc^{-1} and a slowly rotating spiral pattern in the solar neighborhood with $\Omega_{\rm sp} \simeq 25$ km s^{-1} kpc^{-1}. This suggests that there is no dynamical connection between the central bar and the spiral structure, at least on the periphery of our Galaxy.

Note yet another approach to determining the corotation radius associated with the presumed correlation between the peculiarity of the radial metal-

licity distribution $Z(r)$ in the Galactic disk (a local minimum and a plateau) and the position of the corotation radius, which follows, in particular, from chemical-dynamical models for the evolution of galaxies (Mishurov et al. 2002). For our Galaxy, in addition to the pattern speed of the rapidly rotating bar, the profile $Z(r)$ points to a corotation radius $r_c \sim R_\odot$ and a spiral pattern speed $\Omega_{sp} \sim 25-35$ km s^{-1} kpc^{-1} (Mishurov et al. 2002; Acharova et al. 2010). Observational data for open star clusters, given their age, suggest that the corotation radius is close to the position of the solar orbit in the Galaxy, $r_c/R_\odot = 1.06 \pm 0.08$ (Dias and Lépine 2005). This approach allows the position of the corotation radius on the periphery of the stellar disk to be determined from observational data, for example, $r_c/R_{opt} = 0.83$ for IC 0167, $r_c/R_{opt}^{NGC\ 1042} = 0.65$, $r_c/R_{opt}^{NGC\ 6907} = 1.0$ (Scarano et al. 2011); all three galaxies are late-type ones with a bar, with the corotation radius being at its ends. Note also that the approaches by Scarano et al. (2011) and Buta and Zhang (2009) give close values for NGC 1042, $r_c/R_{opt}^{NGC\ 1042} = 0.65$ and 0.6, respectively. The observations of young objects in the vicinity of a spiral arm (Grosbol and Dottori 2009) point to the position of the corotation radius $r_c = 240''$ near the optical radius $R_{opt} = 270''$ for NGC 2997; a well-defined system of rows can be seen in this galaxy.

The rows starting directly from one bar end that form a ringlike spiral going to the other bar end are a peculiarity of several barred galaxies. NGC 1097, NGC 2523, and NGC 4902 are typical representatives. In numerical N-body models, separate straightened arm segments can be seen at the transient formation stage of the bar and spirals (Buta and Combes 1996).

Note also the theoretical spiral structure models indicative of a peripheral position of the corotation radius (Contopoulous and Grosbol 1986). Such models based on the 4/1 resonance allow the observed peculiarities of spiral galaxies to be described (Patsis et al. 1997). As another example, we can point to the dynamics of a galactic disk in a nonaxisymmetric massive dark halo (Khoperskov et al. 2007). A slowly rotating two-armed spiral wave with the corotation located in the outer disk is generated in such models. The conclusion that the corotation radius is on the periphery of the spiral pattern in an appreciable number of galaxies is important for the results of our numerical simulations obtained here, because the galactic shock is straightened most easily in the case of a slowly rotating spiral pattern where the corotation is on the disk periphery.

Sample of Galaxies with Rows

In addition to the catalog of 200 galaxies with rows published by Chernin et al. (2001a), we identified 102 more spiral galaxies with typical PS fragments traceable in their images (see Fig. 1). We used data from LEDA, NED, Pohlen and Trujillo (2006), and SDSS to construct the sample.

In a number of galaxies, the rows can be identified even by old stars (e.g., based on 2MASS data): NGC 2523 and NGC 5653. Such objects are rare, but polygonality in them is revealed by several components.

The goal of this paper is to investigate the possibility of PS generation in the gaseous disks of spiral galaxies by taking into account the following factors:

(1) the gravitational potential of a radially inhomogeneous spiral density wave in the stellar disk;

(2) the solid-body rotation of the spiral stellar disk structure;

(3) the differentiality of the gas rotation;

(4) the radial inhomogeneity of the gaseous disk parameters;

(5) the vertical gas motions.

The listed factors are new compared to those investigated by Chernin et al. (2006) and they allow the most significant observed morphological features of rows in the spiral patterns of several galaxies to be reproduced.

GASDYNAMIC MODEL

The flow of gas in the external potential of a stellar disk and a dark halo is described by the equations of classical gas dynamics. We will assume that the gas is ideal and polytropic with an adiabatic index close to unity, $1 < \gamma < 1.1$. This ensures an efficient allowance for cooling within the framework of a single-component model. We neglect the gas self-gravity effects. The system of gas-dynamic equations can then be written as

$$\frac{\partial \varrho}{\partial t} + \nabla \cdot (\varrho \mathbf{u}) = 0, \quad (1)$$

$$\frac{\partial \varrho \mathbf{u}}{\partial t} + \nabla \cdot (\varrho \mathbf{u} \otimes \mathbf{u}) = -\nabla p - \varrho \nabla \Psi,$$

$$\frac{\partial E}{\partial t} + \nabla \cdot ([E + p]\mathbf{u}) = -\varrho \mathbf{u} \cdot \nabla \Psi,$$

where ϱ is the gas volume density, p is the pressure, $\mathbf{u} = \{u, v, w\}$ is the gas velocity vector, and Ψ is the external gravitational potential. The bulk energy and the internal specific energy are defined, respectively, by the expressions

$$E = \varrho \left(e + \frac{\mathbf{u}^2}{2} \right), \quad e = \frac{p}{\varrho(\gamma - 1)}.$$

Following Wada and Koda (2001), Cox and Gomez (2002), Shetty and Ostriker (2006), we will represent the external potential as the sum of two parts: an axisymmetric one Ψ_0 attributable to the halo and an axisymmetric distribution of matter in the stellar disk and a nonaxisymmetric one associated with the density wave in the stellar disk. It is then convenient to write the potential as

$$\Psi(r,\varphi,z) = \Psi_0(r,z)[1+\varepsilon_0\Psi_1(\xi_\mathrm{s})\cos\Theta_\mathrm{p}], \quad (2)$$
$$\Psi_1 = \frac{\xi_\mathrm{s}^2}{(1+\xi_\mathrm{s}^2)^{3/2}},$$

where

$$\xi_\mathrm{s} = \sqrt{(r/b)^2+(z/h_*)^2},$$
$$\Theta_\mathrm{p} = m\left[\varphi-\varphi_\mathrm{p}(r_0)+\Omega_\mathrm{p}t-\frac{\ln(r/r_0)}{\tan i}\right],$$

b and h_* are the radial and vertical scale lengths, respectively, m is the number of spirals, i is the spiral pitch angle, Ω_p is the spiral pattern speed, and ε_0 characterizes the depth of the potential well for the spiral density wave. In our calculations, we took the following dimensionless parameters: $b=1$, $h_*=0.1$, $r_0=0.9$. For the exponential scale length of an axisymmetric stellar disk with a radial surface density profile $\sigma_*\propto\exp(-r/L_*)$, we assumed that $L_*=0.5$. Thus, the optical radius of the model galaxy is $R_\mathrm{opt}\simeq 4L_*=2$. For this choice of dimensionless parameters, the disk revolution period at radius R_opt is $\tau(r=2)\simeq 6$. The potential of a quasi-isothermal halo provides a plateau-type curve far from the disk center. We will assume that the relative mass of the dark halo within the optical radius is a factor of 1.5–3 larger than the mass of the disk subsystem (stars + gas) (Zasov et al. 2004; Khoperskov et al. 2010).

The system of equations (1) was integrated numerically in a reference frame rotating with the spiral pattern speed Ω_p. For our computer simulations of gaseous disks, we implemented a finite-volume numerical TVD MUSCL scheme (van Leer 1979; Harten 1983) of the second order in time and the third order in space in Cartesian, polar, and cylindrical coordinate systems. The TVD method is efficient for describing an essentially nonstationary flow in which a system of small-scale shocks is formed (Khoperskov et al. 2003). The size of the computational region in 2D models reached 15×15 in the Cartesian coordinate system, while the outer boundary in the polar coordinate system was located at radius $r_\mathrm{max}=7$. To eliminate the numerical boundary effects in the fictitious cells of the computational region, we assumed the gas parameters to be equal to the analytical ones or the gaseous disk to be immersed into a vacuum over the entire computation time. To use the latter alternative, we developed and implemented an approach that allowed the evolution of the matter–vacuum boundary to be computed in numerical models (Eremin et al. 2010).

At the initial time, we assumed that the gas surface density was in the form of a power law:

$$\sigma(r,t=0) = \frac{1}{[1+(r/L_\sigma)^2]^{5/2}},$$

where $L_\sigma\simeq 1$–2 is the spatial scale, and that the isentropic condition was met:

$$p(r,z,t=0) = K\varrho^\gamma(r,z,t=0),$$
$$K=\mathrm{const}.$$

The radial profiles of the flow parameters in the equatorial $z=0$ plane were determined from the conditions for the gaseous disk being axisymmetric and equilibrium for $\varepsilon_0=0$. For 3D models, the disk at the initial time was assumed to be also in a state of hydrostatic equilibrium in the vertical direction.

The numerical grids are determined by the number of cells in the radial, N_r, azimuthal, N_φ, and vertical, N_z, directions. For our 2D simulations, we used several groups of models: $N_r=500$–3200, $N_\varphi=360$–1080. In our 3D simulations, the parameters of the numerical grid are $N_r=1000$, $N_\varphi=360$, $N_z=400$. In the best models as applied to a typical galaxy with $R_\mathrm{opt}=10$ kpc, the corresponding spatial resolution reaches ~10 pc and the angular resolution in azimuth reaches $\Delta\varphi=(1/3)^\circ$.

The main parameters of our numerical models are the amplitude ε_0 responsible for the depth of the spiral potential well, the spiral pitch angle i, the spiral pattern speed Ω_p, and the speed of sound $c_\mathrm{s}\simeq\sqrt{K}$ in the plateau region of the rotation curve. It is convenient to use the effective Mach number $\mathcal{M}_0=V_\mathrm{max}/c_\mathrm{s}^\mathrm{max}$ to characterize the initial temperature in the disk.

THE FORMATION OF POLYGONAL STRUCTURES

Our numerical simulations reveal several stages of gaseous disk evolution in the course of which the formation of PSs is observed (Fig. 2).

At the first stage, smooth spiral shocks are formed on one of the slopes of the potential well: inside the corotation radius (Fig. 3), these shocks are located at the leading (with respect to the onflowing gas) edge of the spiral potential well (line S01 in Fig. 3c) produced by stellar density waves; outside the corotation radius, the shocks are at the trailing edge of the potential well (line S02).

At the second stage, small-scale perturbations giving rise to spurs develop fairly rapidly due to the wiggle instability of shocks (Fig. 4). The small-scale

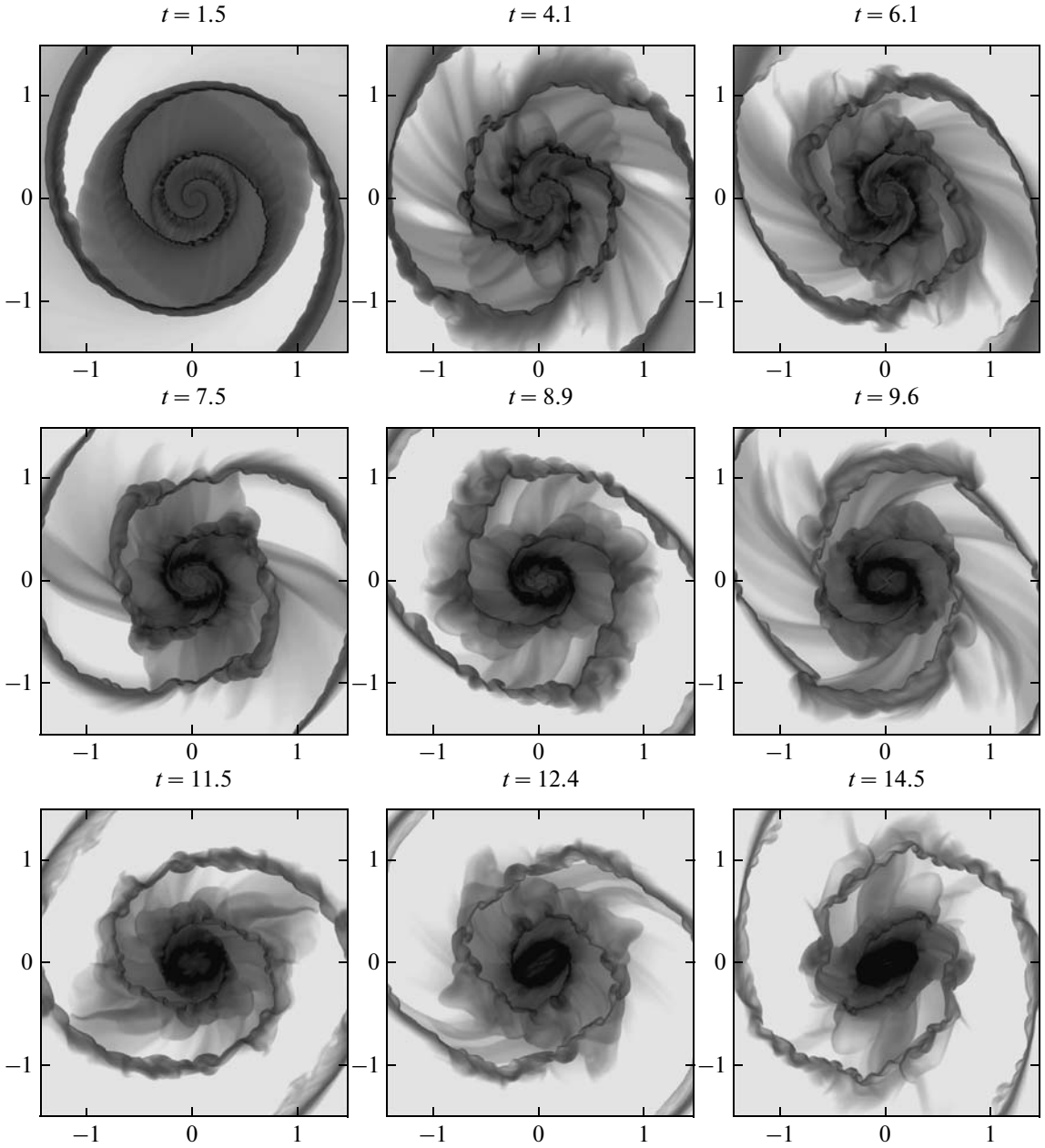

Fig. 2. Evolution of the gaseous disk in the model with $i = 15^\circ$ and $\varepsilon_0 = 0.15$. The logarithm of the surface density at various instants of time t.

irregular features in Fig. 2 are clearly traceable starting from $t = 1.5$. This stage can be absent at certain parameters. The density nodes are clearly seen in Fig. 4b; the nonlinear wave and the "fish fins" moving off the spiral wave at an angle close to 90° consist of their sequence. The formation of spurs in the spiral pattern (the galaxies M51 and M81 are classical examples) through the development of a nonlinear wiggle instability stage was considered by Wada and Koda (2001) and Wada (2008). The formation of a small-scale structure of spirals turns out to be also possible in MHD models (Shetty and Ostriker 2006) through the development of gravitational instability (Shetty and Ostriker 2008) when the thermal effects are taken into account (Dobbs and Bonnell 2006; Kim et al. 2008).

At the third stage, the effect of spiral shock escape from the potential well is observed and the straightening of shock segments giving rise to polygonal structures (rows) in the gaseous disk emerges under certain conditions to be discussed below (see Figs. 2, 3c, 5). Such straight fragments generally follow the geometry of the stellar spiral density wave that is determined by the nonaxisymmetric part of potential (2).

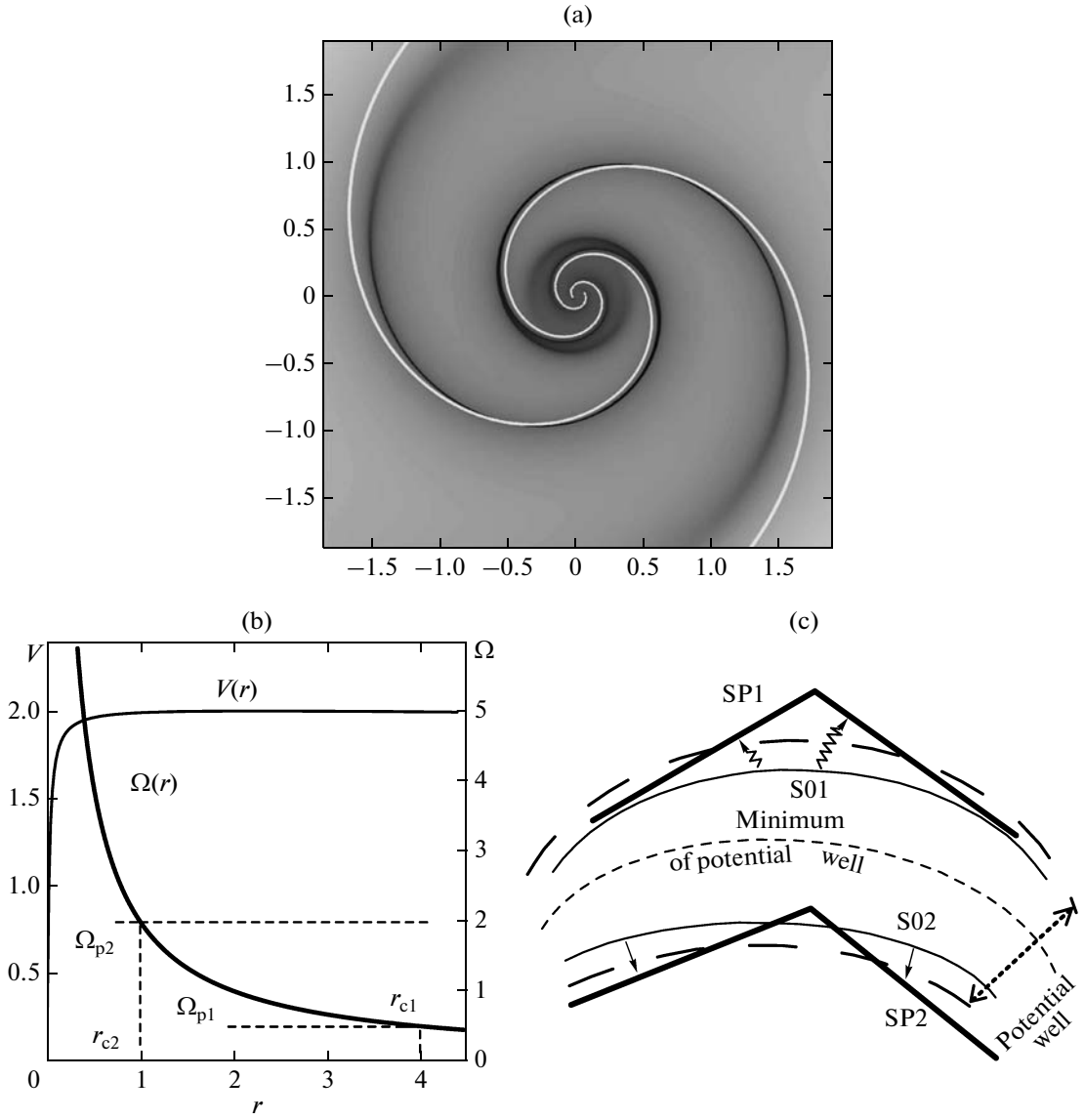

Fig. 3. (a) Position of the shock (the darkest color) in the potential well of a spiral density wave (the white line specifies the position of the minimum of the potential well for potential (2)). The corotation radius $r_c = 1$. (b) Radial dependences of the rotation velocity $V(r)$ and angular velocity $\Omega(r)$ for the gas. For the angular velocity Ω_{p1}, the corotation is on the disk periphery ($r_c = 4$). The case of Ω_{p2} and r_{c2} corresponds to Fig. 3a. (c) The scheme of shock positions in the potential well of a spiral density wave.

The evolution of the spiral structure in gas is peculiar in that it is nonstationary—the rows do not form any stationary pattern, which is additionally complicated by the system of spurs whose properties change on short time scales compared to the disk revolution period.

The shock escape from the potential well in the constructed models turns out to be possible only if the shock is on the outer slope of the potential well (see S01 in Fig. 3c)—the transition to position SP1 occurs. The transition of shock S02 from the inner slope of the potential well to the polygonal geometry SP2 turns out to be impossible. The former situation (S01 → SP1) corresponds to the outer corotation radius r_{c1} (see Fig. 3b), while the latter situation corresponds to fast rotation of the spiral pattern with r_{c2}. Thus, in the purely hydrodynamic model being discussed here, the position of the corotation radius on the disk periphery is a necessary condition for the emergence of PSs.

The described result differs from the conclusion reached in Chernin et al. (2006), where case SP2

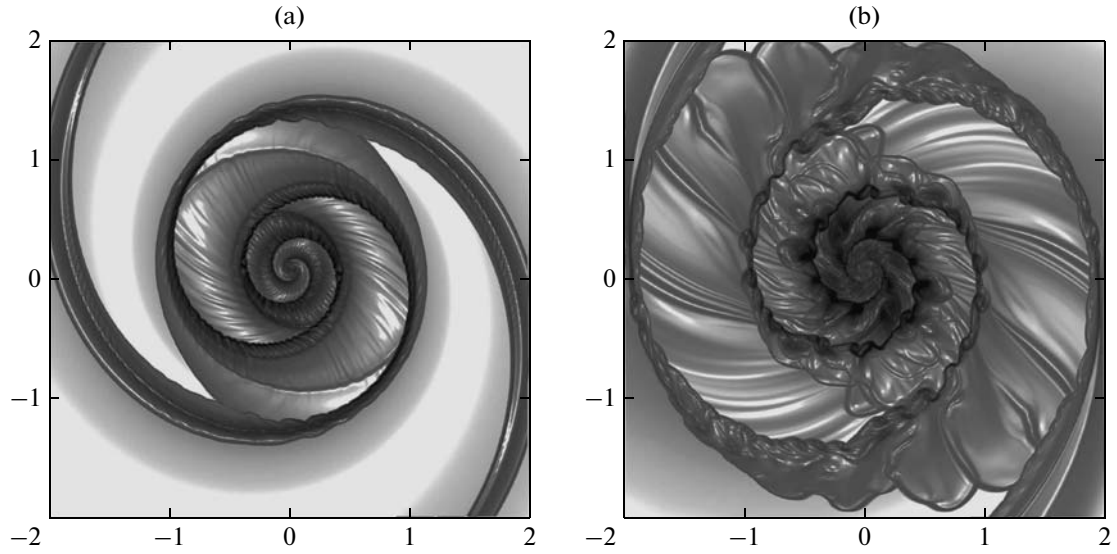

Fig. 4. The model with $\varepsilon_0 = 0.15$, $\mathcal{M}_0 = 30$, $i = 15^\circ$, and $r_c = 4$. (a) The initial stage of wiggle instability development. (b) The stage of developed spurs. A special method is used for visualization: the surface of the function $z = \sigma(x, y)$ is shown in the presence of illumination, which enhances the contrast.

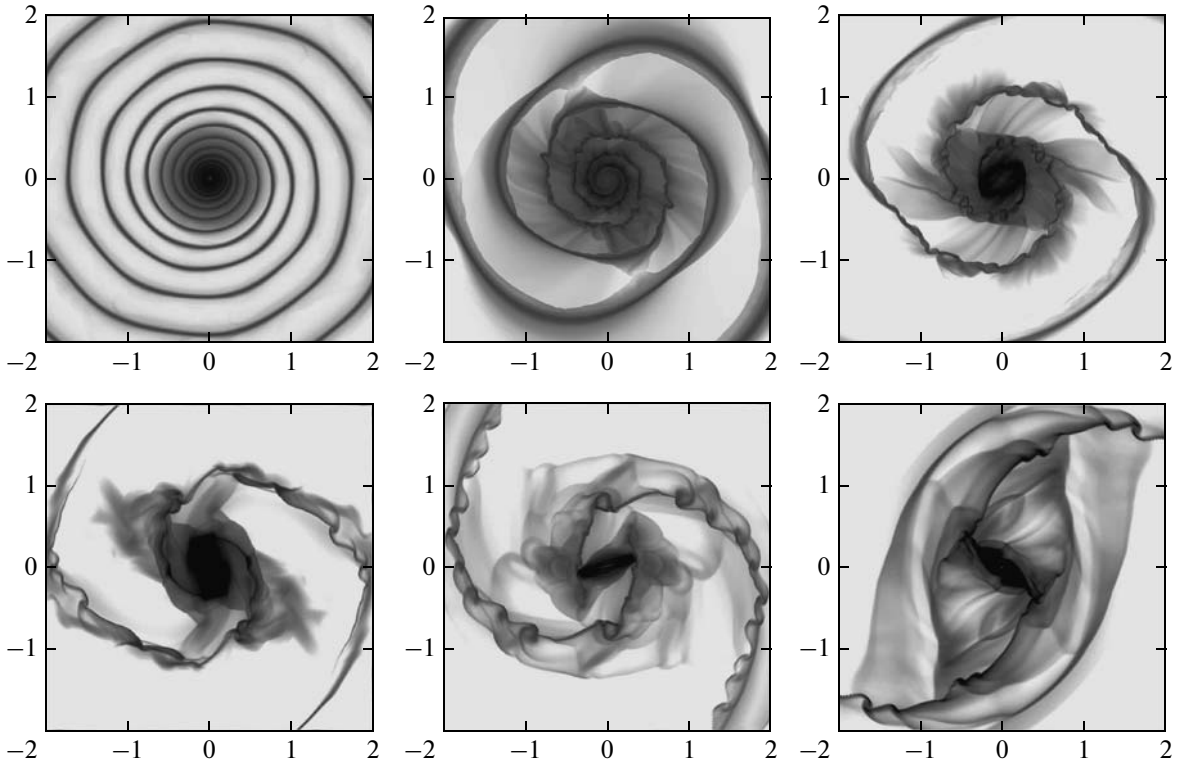

Fig. 5. PSs in the models with $\varepsilon_0 = 0.1$, $\mathcal{M}_0 = 30$, $r_c = 4$ for various pitch angles $i = 5^\circ, 10^\circ, 15^\circ$ (upper row); $i = 20^\circ, 30^\circ, 50^\circ$ (lower row).

is realized (see Fig. 3c). The consideration of only a plane flow in Chernin et al. (2006) without any allowance for disk rotation, radial inhomogeneities of the spiral potential and gas density, and rotation differentiality is responsible for this difference. Including the latter factors changes radically the position of the shock front in the potential well. In the plane problem, the shock is at the entrance of a supersonic flow into

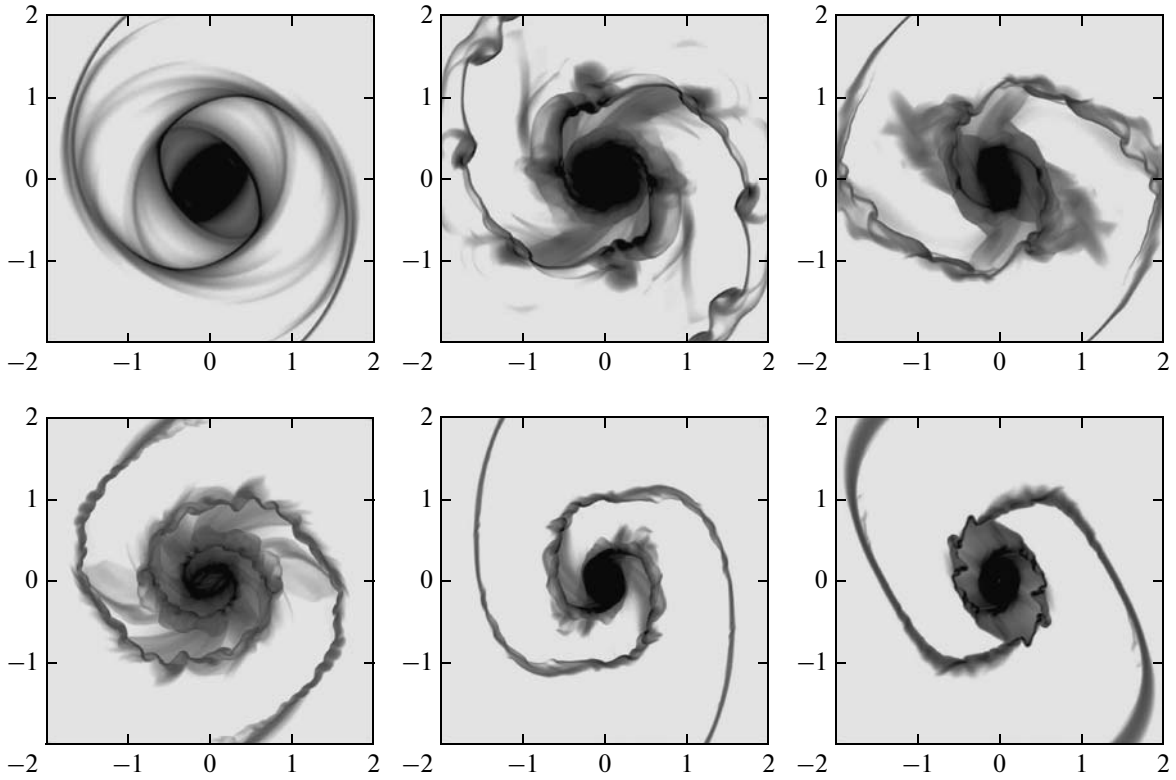

Fig. 6. The models with $i = 20^\circ$, $\mathcal{M}_0 = 30$, $r_c = 4$ for various values of $\varepsilon_0 = 0.01, 0.05, 0.1$ (upper row); $\varepsilon_0 = 0.15, 0.2, 0.3$ (lower row).

the potential well. In the realistic model of a rotating gaseous disk and a spiral stellar density wave, the shock is at the exit from the potential well.

We constructed a series of models with various spiral pitch angles i (see Fig. 5). At any values of i in our numerical simulations, we can identify the time intervals with well-defined rows even for a small amplitude of the stellar density wave, $\varepsilon_0 = 0.1$. At small pitch angles (see the case of $i = 5^\circ$ in Fig. 5), the formation of PSs is not accompanied by the development of wiggle instability.

The amplitude of the stellar spiral density wave ε_0 affects significantly the formation of the spiral structure in the gas subsystem (Fig. 6). The amplitude of the stellar spiral density wave affects in a complex way the PS generation efficiency. On the one hand, the wave amplitude in gas increases with ε_0. On the other hand, it is easier for the shock to escape from a shallow shock potential well, which is necessary for the formation of straightened segments of perturbations. As we see, the former factor plays a more important role for the formation of PSs. In a deeper potential well (at larger ε_0), we obtain more pronounced kinks of the shock front in the gas component. At a small amplitude $\varepsilon_0 \lesssim 0.01$, no rows are formed in our simulations (see Fig. 6).

The transient nature of PSs is a characteristic feature of the constructed numerical models. Their parameters (the positions of kinks, the lengths of rows, the angle between them, and even their number) change with time. Having emerged after the shock escape from the potential well, the PSs begin to weaken, almost disappearing, and the rows are subsequently restored again. In the case of a deeper potential well, the rows live over longer time intervals. The generation of PSs is determined by the physics of shocks in a spiral gravitational well, which begin to evolve due to the development of shear instability.

The constructed models are not self-consistent, because no allowance is made for the reverse effect of the gas on the geometry of the spiral pattern in the stellar component. In the case of such an allowance, one would expect an enhancement of the transient character of PSs.

On the whole, our 3D simulations in the cylindrical coordinate system on a grid with a resolution $\Delta r \times \Delta\varphi \times \Delta z = 0.01 \times 1^\circ \times 0.01$ confirm the results of our 2D models (Fig. 7). Transient PSs are formed in the same way.

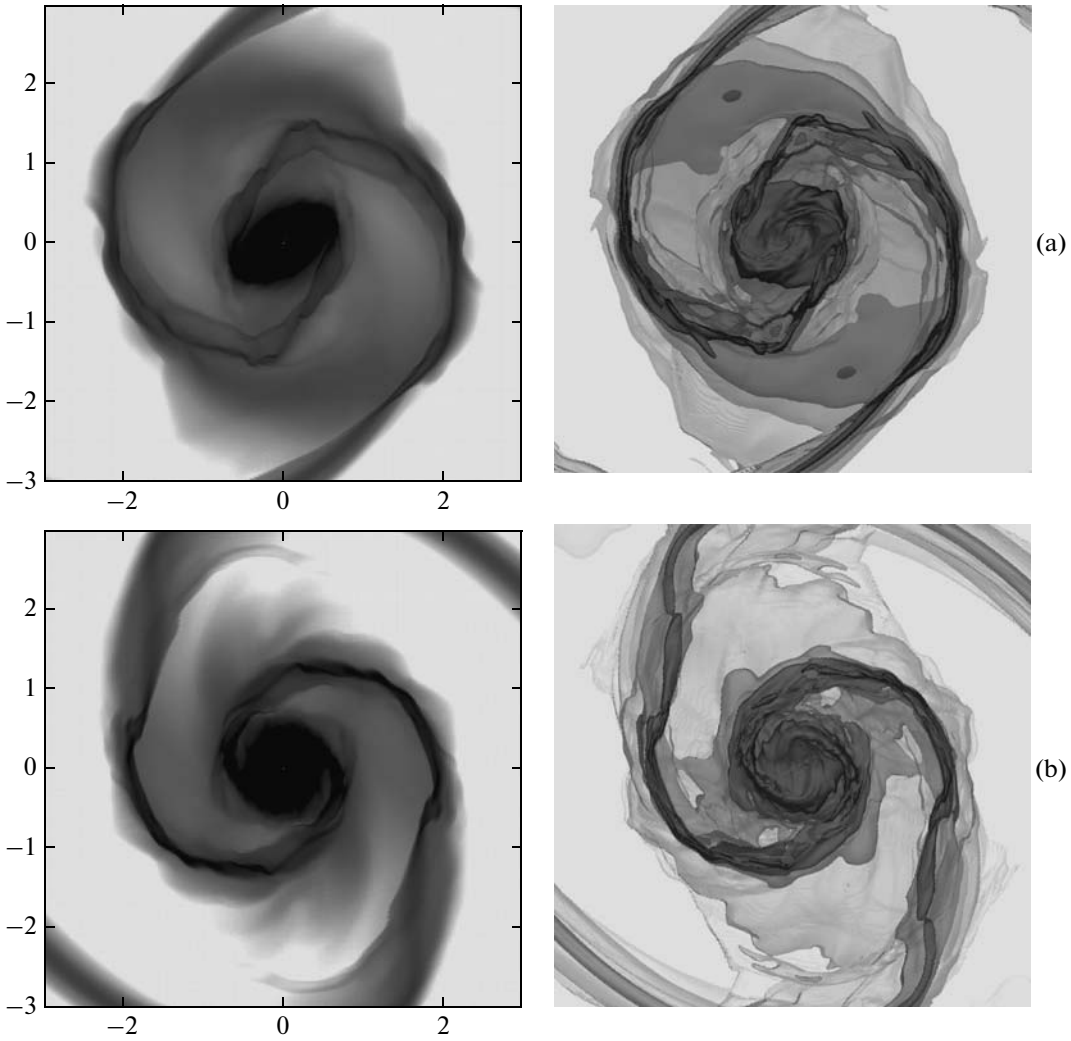

Fig. 7. The structure of a 3D gaseous disk in the presence of rows at two different instants of time (a, b): the surface density is on the left; the isosurfaces of the logarithm of volume density are on the right.

PARAMETERS OF POLYGONAL STRUCTURES

The formation of straightened segments of spiral shocks depends on model parameters. Let us discuss the pattern of this influence.

First, the number of PSs depends on the spiral pitch angle. At small pitch angles, $i = 5°–20°$, the number of straightened segments is great (typically five–seven or more). At large pitch angles, $i \geq 50°$, the number of kinks decreases to one or two.

Second, slow rotation of the spiral pattern at which the corotation radius is on the disk periphery (see Fig. 3) contributes best to the formation of PSs. When $r_c = V(r_c)/\Omega_p \lesssim L_\sigma$, no rows are observed.

Third, the evolution of the gaseous disk is strongly affected by the depth of the spiral potential well ε_0. At low perturbation amplitudes, $\varepsilon_0 \lesssim 0.03$, no wiggle instability develops; nevertheless, the straightening of the spiral shock front turns out to be possible. In models with large depths of the potential well, $\varepsilon \geq 0.25$, almost stationary PSs are formed in the gaseous disk. In this case, not only the shock escape from the potential well but also the spiral shock splitting into two (or occasionally more) branches is observed.

In the models considered, the rows are always located at the outer edge of the potential well—ahead (with respect to the gravitational potential minimum) of the stellar density wave, provided that the corotation radius r_c lies on the disk periphery. In this case, increasing the corotation radius from $r_c = 4$ (Fig. 8a) to $r_c = 20$ (Fig. 8b) retains the possibility of the formation of rows.

Note the influence of the Mach number $\mathcal{M}_0$ on PS properties. All other things being equal, fast

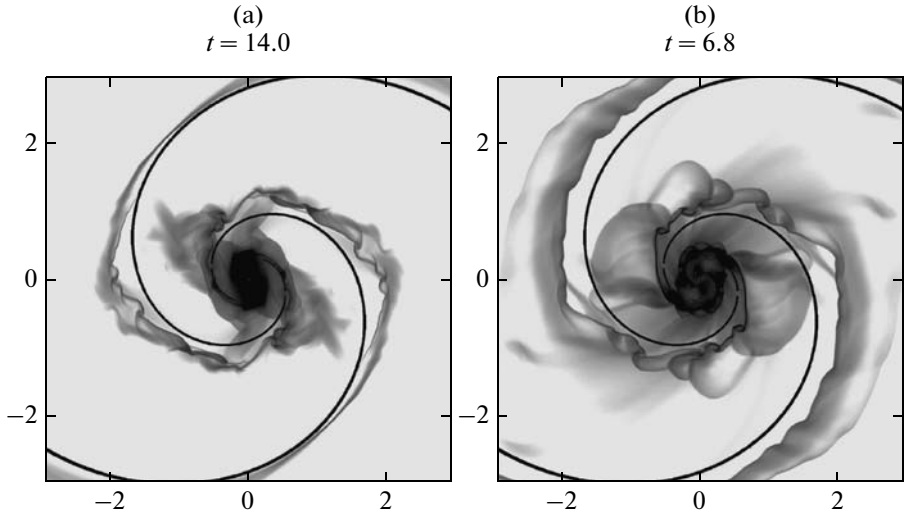

Fig. 8. PS positions relative to the minimum of the potential well from the spiral arm of the stellar component (solid lines). The models with $\mathcal{M}_0 = 30$, $i = 20°$, $\varepsilon_0 = 0.1$, $\Omega_p = 0.5$ (a), $\Omega_p = 0.1$ (b).

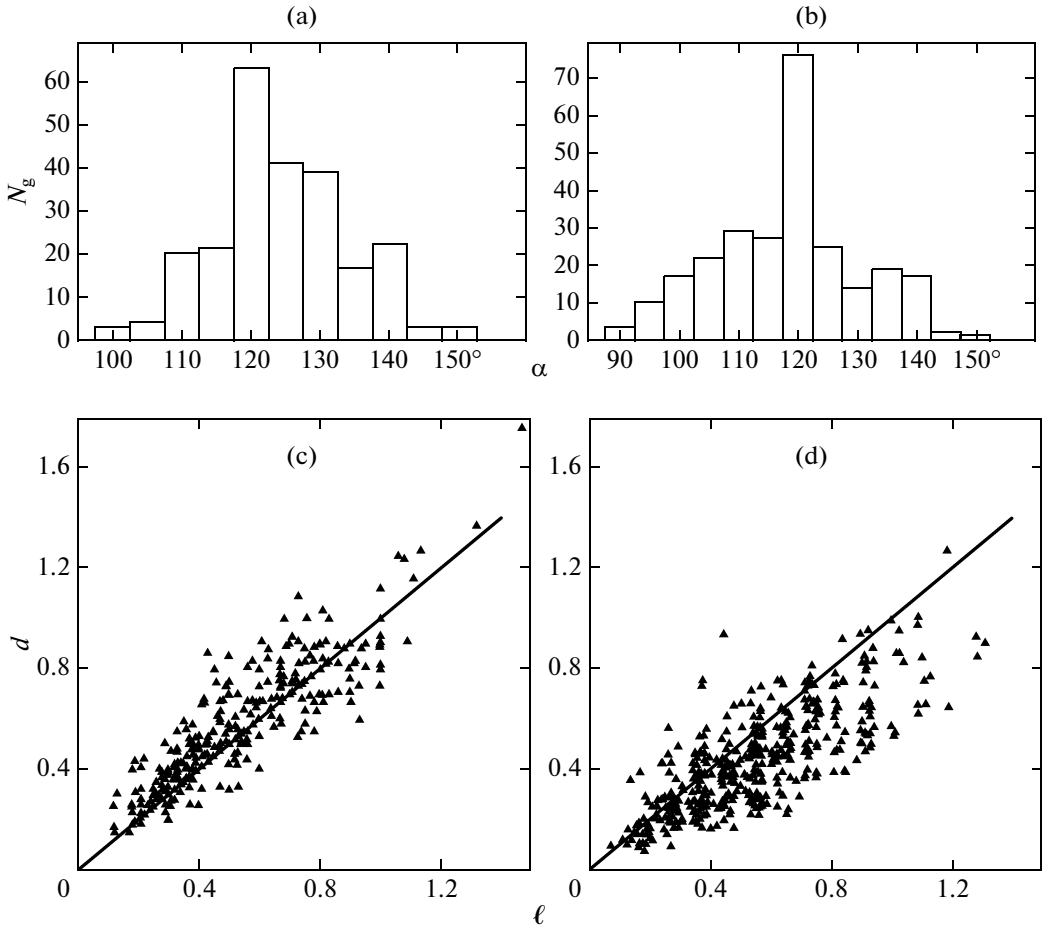

Fig. 9. Results of the statistical analysis of observational data for a sample of stars (Chernin et al. 2001a) (a, c) and for a series of numerical simulations at various instants of time at the stage with a developed system of rows (b, d): (a, b) Histograms of the number of straightened segments versus angle α between them; (c, d) length ℓ of a straightened segment versus distance d to the disk center. The solid line: $d = a\ell + b$ obtained by Chernin et al. (2001a).

disk rotation (large $\mathcal{M}_0$) contributes to the formation of PSs. At effective Mach numbers $\mathcal{M}_0 \lesssim 10$, the conditions for the development of wiggle instability deteriorate. This, in turn, makes the shock escape from the gravitational well of a stellar density wave difficult, which is necessary for the formation of an extended straightened segment of the gaseous pattern. If we take $c_s \sim 10-15$ km s^{-1}, then we have $V_{max} \simeq 100-150$ km s^{-1} for $\mathcal{M}_0 = 10$. Note that rows are encountered very rarely among slowly rotating galaxies.

Figure 9 shows the PS parameters from more than 40 numerical simulations in comparison with the observational data for 200 galaxies (Chernin et al. 2001a). For each simulation, we chose several instants of time with a developed system of rows. The total number of measurements was 450. The histograms of the number of straightened spiral arm segments N_g versus angle between neighboring segments α are shown at the top. As we see, the maximum in the distribution occurs at an angle of 120°, in complete agreement with the observational data. The number of pairs of rows with $\alpha = 120° \pm 2.5°$ in our numerical simulations was 30% of the total number.

The size of a straightened spiral segment depends on Galactocentric distance linearly, but the slope of the straight line turns out to be slightly different from the value obtained by processing the observational data in Chernin et al. (2000). This difference may stem from the fact that we used a cube of models with a uniform step in parameters $i, \varepsilon_0, \mathcal{M}_0$, while the sample of galaxies definitely does not cover uniformly the grid of parameters $(i, \varepsilon_0, \mathcal{M}_0)$. On the other hand, we did not consider spiral patterns with $m > 2$ arms, while a significant fraction of the total number of objects with rows in the sample of galaxies is accounted for by multiarmed patterns.

Significantly, the PS formation mechanism considered here is purely hydrodynamic and is associated with an unstable location of the shock front in the spiral potential well.

CONCLUSIONS

In conclusion, let us formulate our main results:

(1) We showed that PSs could be formed in the gas component in a simple hydrodynamic model due to an unstable position of the shock front in a spiral stellar density wave. Numerical models with high spatial and temporal resolutions are needed to generate these features.

(2) We showed that PSs could be formed for pitch angles of the spiral pattern 5°–50°.

(3) As a rule, the system of rows in the numerical models is essentially nonstationary.

(4) The characteristic formation time of straightened segments does not exceed the revolution period of the stellar disk periphery.

(5) PSs emerge in models with a slowly rotating spiral pattern when the corotation radius is on the disk periphery.

(6) The results of our 2D and 3D gaseous disk simulations are in good agreement.

(7) The geometric properties of rows in the models agree well with the processing results for observed spiral patterns. In particular, the predominant angle between segments is $\alpha \simeq 120°$.

The increase in the fraction of galaxies with PSs among the interacting ones probably stems from the fact that an external gravitational effect facilitates the escape of a galactic shock from the potential well of a stellar arm, facilitating the shock straightening.

ACKNOWLEDGMENTS

We wish to thank A.V. Zasov, V.I. Korchagin, and A.D. Chernin for useful discussions. The numerical simulations were performed on the "Chebyshev"supercomputer of the Moscow State University with assistance from A.V. Zasov and N.V. Tyurina. This work was supported (project no. 10-07-97017-Povolzh'e) in part by the "Scientific and Scientific-Pedagogical Personnel of Innovational Russia" Federal Goal-Oriented Program (P1248).

REFERENCES

1. I. A. Acharova, J. R. D. Lepine, Yu. N. Mishurov, et al., Mon. Not. R. Astron. Soc. **402**, 1149 (2010).
2. R. J. Buta and X. Zhang, Astrophys. J. Suppl. Ser. **182**, 559 (2009).
3. R. Buta and F. Combes, Fund. Cosmic Phys. **17**, 95 (1996).
4. R. Buta and G. B. Purcell, Astron. J. **115**, 484 (1998).
5. S. Chakrabarti, G. Laughlin, and F. H. Shu, Astrophys. J. **596**, 220 (2003).
6. A. D. Chernin, Astrophys. **41**, 399 (1998).
7. A. D. Chernin, Mon. Not. R. Astron. Soc. **308**, 321 (1999a).
8. A. D. Chernin, Pis'ma Astron. Zh. **25**, 684 (1999b) [Astron. Lett. **25**, 591 (1999)].
9. A. D. Chernin, A. V. Zasov, V. P. Arkhipova, and A. S. Kravtsova, Pis'ma Astron. Zh. **26**, 342 (2000) [Astron. Lett. **26**, 285 (2000)].
10. A. D. Chernin, A. S. Kravtsova, A. V. Zasov, and V. P. Arkhipova, Astron. Zh. **78**, 963 (2001a) [Astron. Rep. **45**, 841 (2001)].
11. A. D. Chernin, A. V. Zasov, V. P. Arkhipova, et al., ASP Conf. Ser. **230**, 147 (2001b).
12. A. D. Chernin, A. V. Zasov, V. P. Arkhipova, et al., Astron. Astroph. Trans. **20**, 139 (2001c).
13. A. D. Chernin, V. V. Korolev, and V. V. Kovalenko, Astrophys. Space Sci. Lib. **337**, 321 (2006).

14. G. Contopoulous and P. Grosbol, Astron. Astrophys. **155**, 11 (1986).
15. D. P. Cox and G. C. Gomez, Astrophys. J. Suppl. Ser. **142**, 261 (2002).
16. W. S. Dias and J. R. D. Lépine, Astrophys. J. **629**, 825 (2005).
17. C. L. Dobbs and I. A. Bonnell, Mon. Not. R. Astron. Soc. **367**, 873 (2006).
18. Yu. N. Efremov, Pis'ma Astron. Zh. **35**, 563 (2009) [Astron. Lett. **35**, 507 (2009)].
19. Yu. N. Efremov, Mon. Not. R. Astron. Soc. **405**, 1531 (2010).
20. Yu. N. Efremov, Astron. Astroph. Trans. **20**, 115 (2001).
21. Yu. N. Efremov and A. D. Chernin, Usp. Fiz. Nauk **173**, 3 (2003) [Phys. Usp. **46**, 1 (2003)].
22. B. G. Elmegreen, Astrophys. J. **242**, 528 (1980).
23. B. G. Elmegreen, E. Wilcots, and D. J. Pisano, Astrophys. J. Lett. **494**, 37 (1998).
24. M. A. Eremin, A. V. Khoperskov, and S. A. Khoperskov, Izv. VolGTU, Aktual. Probl. Upravl., Vychisl. Tekhn. Informat. **13**, 24 (2010).
25. O. Gerhard, arXiv1003.2489 (2010).
26. P. Grosbol and H. Dottori, Astron. Astrophys. **499**, 21 (2009).
27. A. Harten, J. Comput. Phys. **49**, 357 (1983).
28. A. V. Khoperskov, M. A. Eremin, M. A. Butenko, and S. S. Khrapov, Vestn. Volgogr. Gos. Univ., Ser. Matem. Fiz. **11**, 105 (2007).
29. A. V. Khoperskov, S. S. Khrapov, and E. A. Nedugova, Pis'ma Astron. Zh. **29**, 288 (2003) [Astron. Lett. **29**, 246 (2003)].
30. A. Khoperskov, D. Bizyaev, N. Tiurina, et al., Astron. Nach. **331**, 731 (2010).
31. Ch.-G. Kim, W.-T. Kim, and E. C. Ostriker, Astrophys. J. **681**, 1148 (2008).
32. LEDA, HyperLeda, http://leda.univ-lyon1.fr/.
33. B. van Leer, J. Comput. Phys. **32**, 101 (1979).
34. Yu. N. Mishurov, J. R. D. Lepine, and I. A. Acharova, Astrophys. J. Lett. **571**, 113 (2002).
35. K. Muraoka, K. Kohno, T. Tosaki, et al., Astrophys. J. **706**, 1213 (2009).
36. NED, NASA–IPAC Extragalactic Database—NED, http://ned.ipac.caltech.edu/.
37. P. A. Patsis, P. Grosbol, and N. Hiotelis, Astron. Astrophys. **323**, 762 (1997).
38. M. Pohlen and I. Trujillo, Astron. Astrophys. **454**, 759 (2006).
39. P. Rautiainen, H. Salo, and E. Laurikainen, Mon. Not. R. Astron. Soc. **388**, 1803 (2008).
40. S. Scarano, J. Lepine, and M. Marcon-Uchida, Mon. Not. R. Astron. Soc. (in press) arXiv:1012.5794 (2011).
41. SDSS, NGC Galaxies in the SDSS Data Release 2 (DR2), http://www.sdss.org/dr2/.
42. R. Shetty and E. C. Ostriker, Astrophys. J. **647**, 997 (2006).
43. R. Shetty and E. C. Ostriker, Astrophys. J. **684**, 978 (2008).
44. O. K. Sil'chenko and A. V. Moiseev, Astronom. J. **131**, 1336 (2006).
45. M. A. la Vigne, S. N. Vogel, and E. C. Ostriker, Astrophys. J. **650**, 818 (2006).
46. B. A. Vorontsov-Vel'yaminov, Astron. Zh. **41**, 814 (1964) [Sov. Astron. **8**, 649 (1964)].
47. B. A. Vorontsov-Vel'yaminov, *Extragalactic Astronomy* (Nauka, Moscow, 1977; Harwood Acad., 1987).
48. K. Wada, Astrophys. J. **675**, 188 (2008).
49. K. Wada and J. Koda, Publ. Astron. Soc. Jpn. **53**, 1163 (2001).
50. W. H. Waller, R. C. Bohlin, R. H. Cornett, et al., Astrophys. J. **481**, 169 (1997).
51. A. V. Zasov, A. V. Khoperskov, and N. V. Tyurina, Pis'ma Astron. Zh. **30**, 653 (2004) [Astron. Lett. **30**, 593 (2004)].
52. X. Zhang and R. J. Buta, Astron. J. **133**, 2584 (2007).
53. X. Zhang and R. J. Buta, arXiv:1012.0277 (2010).

Translated by V. Astakhov